High Harmonic Generation via the Non-collinear Optical Gating scheme on plasma surfaces

Tycjan Chironga

December 2019

Contents

1 Abstract

Non-collinear optical gating (NOG) has been proposed as a source of high energy, collimated beams of radiation, via high harmonic generation (HHG), with the possibility of creating individual atto-second pulses using modern tabletop lasers. The scheme relies on two non-collinearly propagating laser pulses interacting with the HHG medium to produce a wave-front rotation at focus. This wave-front rotation should lead to the creation of atto-second pulses, each with a different angle. Although the scheme has only been tested in gases, the underlying concept of wave-front rotation, which creates angularly streaked pulses, has been successfully tested in HHG from plasma surfaces via the atto-second lighthouse scheme. Therefore, there is reason to believe, the similar NOG scheme could apply for both HHG from gases and plasma surfaces.

The primary goal of the study is to report on initial simulations which implement the NOG scheme by using a plasma surface. In these simulations, carried out using the EPOCH particle-in-cell code, two laser pulses separated by an angle 2α, with one of the pulses offset in time by an interval $\pm\Delta t$, will be focused onto overdense plasma. The reflected light containing high order harmonics will be propagated for a set period of time to allow for pulse divergence. The resulting 2D field distributions are analysed mainly via Fourier transform to obtain spectra. By filtering out low frequencies from spectra, the visualisation of atto-second scale pulse train becomes possible in the time domain.

The results find angularly separated pulse trains from harmonics on the order of $20\omega_0$, and upwards. In the frequency domain the pulses are observed as separate bands of intensity at the odd harmonics. It is found that lower harmonics display a large degree of divergence after the HHG interaction, while high frequency harmonics are concentrated close to the optical axis of the simulation, with a maximum angle between the axis and the harmonic band being less than 20 milli-radians. Though the findings show a spatial separation of pulses, the current evidence is insufficient to attribute these to the NOG scheme. Instead plasma surface denting is a more likely candidate, explaining the tight bunching of the created pulses and the small shift in angle between each subsequent pulse which slows as the interaction proceeds. The pulse migration and the decreased effect over time is proposed to be the continued movement of the disturbed plasma surface during reflection. As the pulse envelope passes, the intensity driving the denting decreases and as does the recession velocity of the surface. This results in later pulses having a greater alignment and more consistent propagation direction.

One important point of note is the disagreement of some of the results concerning the propagation angles of pulses allowed to travel further distances. The variance between the propagation angles after could easily be explained by the use of different resolutions for the simulations, with the field spectrum being sampled at $250\mu m$, using a $5k \times 5k$ grid, while the nearer field distribution sampled at $112\mu m$ had ran using a $8k \times 8k$.

Further studies are required to fully asses the feasibility of the NOG scheme and its compatibility with plasma driven HHG. A reduction in the prevalence of denting should, in the ideal case reduce the focusing due surface recession. This may be mediated via increasing the plasma density of the reflecting surface, however this may introduce the added computational toll of increasing the spatial resolution to resolve the plasma frequency ω_p. The other option, which lacks the needs for increased computational resources and prevents excessive denting is a reduction of the peak field intensity. Additional factors, believed to affect the scheme but which have not been tested in this study are the interval between pulses Δt and the carrier-envelope-phase of the pulses. Future studies which tweak these simulation parameters to bring out the behaviour predicted by NOG in

gases are recommended.

2 Introduction

The advent of ultra-short laser pulses made possible by the Chirped Pulse Amplification (CPA) [1] technique has, in recent years, breathed new life into a vast array of fields requiring superb temporal resolution on the femto-second scale as is necessary for time resolved spectroscopy studies into molecular dynamics. Additionally CPA enabled lasers yields unprecedented pulse energies on the order of $10^{22} Wcm^{-2}$ [2] suitable for nuclear fusion research by centres such as the National Ignition Facility [3].

With such a short duration and high peak power the breadth of knowledge pertaining to ultra-fast science in the femto-second ($1fs = 1 \times 10^{-15}s$) regime is ever-expanding, however our understanding of any particular aspect of an ultra-fast process is fundamentally limited by temporal resolution. Thankfully, advances in Physics never truly arrive at a complete standstill and new techniques and novel physical processes allow us to delve into the world of atto-second science ($1as = 1 \times 10^{-18}s$) . In the world of laser physics, however, this is no easy feat, for starters a pulse of duration 200as would require a spectral bandwidth ranging from the near infrared to the extreme ultraviolet [4].

To date few traditional laser systems come close to even approaching the band-with requirement without relying on novel physical phenomena. One promising technique with the potential of opening the doors to atto-second science research is high harmonic generation (HHG), which, when applied in conjunction with femto-second laser pulses can be used to produce bright and coherent sources of extreme UV and soft X-ray light in the form of brief pulses on the order of atto-seconds.

The two competing mechanisms for the generation of short, high frequency, pulses are gas high harmonic generation (more commonly abbreviated as just HHG) and plasma surface harmonic generation (SHHG). In both cases the mechanism leads to the creation of an integer number of harmonics of the driving laser frequency hence fulfilling the most basic requirement for the production of atto-second pulses. Of these the more popular and thoroughly studied method is high harmonic generation in gases where a laser pulse is transmitted through an extended molecular gas medium. The popularity may be attributed to the high conversion efficiency in the extreme-UV and soft x-ray region and ability to produce atto-second pulses using laser intensities of $10^{14} - 10^{15} Wcm^{-2}$ from near-IR sources [5, 6].

With current pulse durations down to $< 100as$ alongside photon and pulse energies of $80eV$ and $0.5nJ$, respectively [7], the allure of gas HHG is obvious. While not the main focus of the study behind this report, gas HHG must be considered as many techniques used to gate the atto-second pulses are applicable to SHHG. In this context gating refers to modifying the temporal and spatial profile of the resulting pulses by using novel experimental geometries. In contrast, SHHG is subject to fewer in depth studies but offers much greater potential over gas HHG which breaks down at intensities above $10^{15} Wcm^{-2}$. Above this intensity the mechanism ceases to produce harmonics due to excessive ionisation of the medium. The mechanism behind SHHG is also fundamentally different from the gas HHG as the incident laser beam is incident onto a solid target, which when ionised by the incoming laser, forms a dense reflective plasma. It is during reflection from this plasma very high order harmonic radiation is produced. In fact, recent experimental studies detect radiation up to the 3200^{th}harmonic [8].

Clearly, in order to develop the next generation E-UV and X-ray sources compatible with current high power, ultra short lasers, a different mechanism such as HHG from plasma surfaces must be

further studied and utilised. The study contained in this report will aim to describe the mechanisms behind harmonic generation from plasma surfaces by performing numerical simulations alongside exploiting alternative interaction geometries as a means of producing individual atto-second pulses suitable for a range of applications such as atto-second pump/probe spectroscopy [5].

The structure of this report is as follows. Section 3 covers the physics behind SHHG and the notable features of the resulting spectrum alongside an explanation behind the origin of atto-second pulses using the technique. Further, it shall briefly introduce the concept of pulse gating with the goal of creating individual atto-second pulses. In section 4 we are introduced to the concept of non-collinear optical gating (NOG) geometry which forces harmonic radiation to be swept across a range of angles. The methodology used to study the concept of NOG via plasma simulations using the EPOCH software is discussed in section 5. Furthermore this section examines some of the limitations of the plasma simulation. Lastly, section 6 discusses the main findings from the simulations.

3 Background

3.1 Surface High Harmonic Generation

Geometry As mentioned in the previous section, surface high harmonic generation occurs when an intense laser pulse of frequency ω_0 and intensity $I > 10^{15} W cm^{-2}$ with a duration on the order of a few tens of femto seconds is incident onto a solid target. Owing to the short duration of the pulse ion dynamics can be neglected due to their comparatively large mass. As the electric field on the surface increases with the rising edge of the pulse, the target becomes becomes ionised, forming an overdense plasma of density n_e at a corresponding plasma frequency ω_p. Classically the plasma frequency can be seen as the rate of gyration of the global plasma frequency,

$$\omega_p = \sqrt{\frac{n_e e^2}{m^* \epsilon_0}}. \tag{1}$$

Here m^* is the effective mass of the electrons in the plasma, e is the electron charge and ϵ_0 is the vacuum permittivity. Provided $\omega_0 \leq \omega_p$ the incident pulse will be reflected. The density at which reflection occurs for a particular frequency is known as the critical density n_c.

Following plasma formation at the surface, the electric and magnetic fields act to perturb the surface in an oscillatory fashion in phase with the driving field. Provided high laser intensities the motion of the reflective surface or plasma mirror, becomes relativistic. The relativistically oscillating mirror model (ROM) explains the production of harmonics as a Doppler shift induced by a reflection from a moving surface. In accordance with classical relativistic theory [9], a pulse of length τ_0 and central frequency ω_0 reflecting off a surface moving at constant velocity v will experience a contraction proportional to γ^2 as given by,

$$\tau' = \frac{\tau_0}{4\gamma^2}, \tag{2}$$

Where γ is the Lorentz factor,

$$\gamma(v) = \frac{1}{\sqrt{1 - \frac{v^2}{c^2}}} \tag{3}$$

Alongside the temporal compression of the pulse, the wave undergoes a blue-shift such that,

$$\omega' = 4\gamma^2\omega_0. \tag{4}$$

In the case of SHHG the velocity of the surface has a sinusoidal dependence due to the driving field i.e. $v(t) \propto sin(\omega_0 t)$. As a result, the gamma factor varies sharply as a function of time as seen in Fig. (1). For a varying γ, the degree of else compression and frequency up shift is different at each point in the cycle, with the maximum velocity corresponding to γ_{max}. It follows that the highest frequencies produced in the reflection only occur for large γ, hence occurring twice every laser cycle.

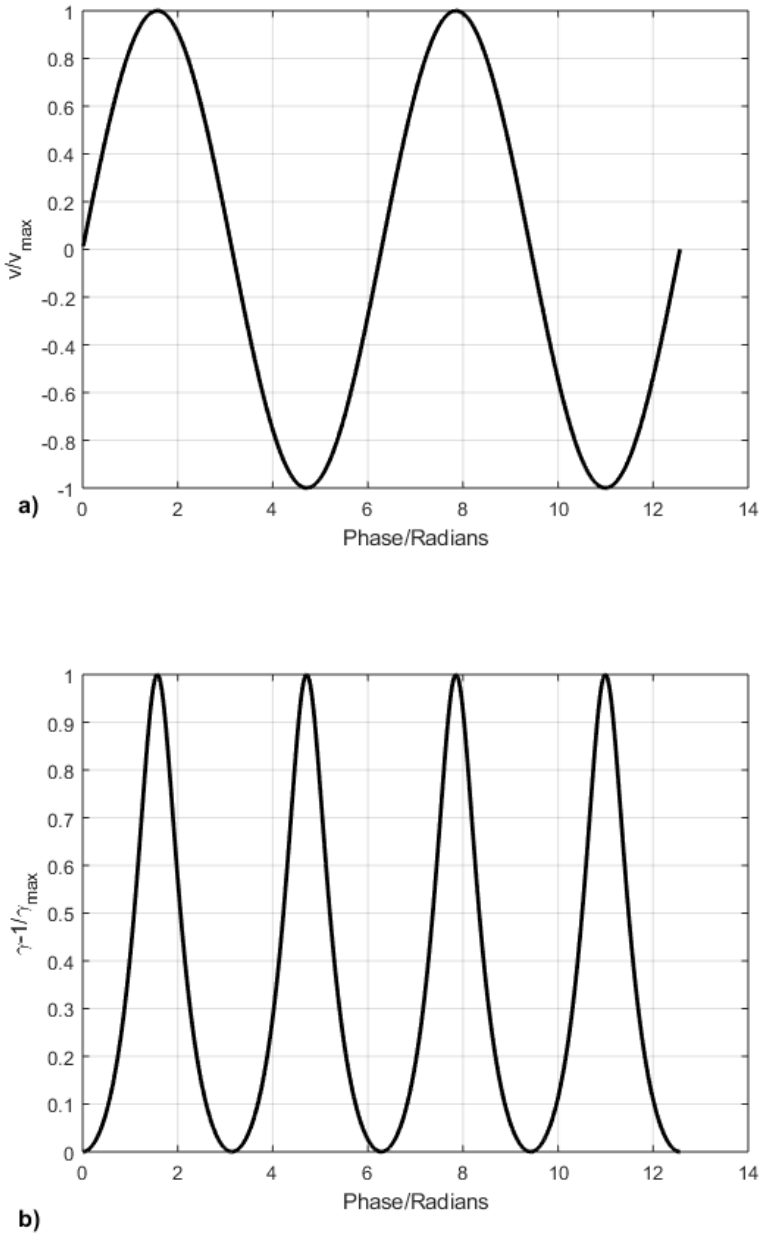

Figure 1: (a) Velocity of the plasma surface represented in the form of a sinusoidal function $[v(\Phi) = v_{max}sin(\Phi)]$ of an arbitrary phase between 0 and 4π. (b) Corresponding plot of the gamma factor in terms of the phase. The plot exhibits a sharp spike for $v = v_{max}$ referred to as a γ-spike.

A more detailed theory behind the ROM model, developed by Gordienko et al [10] and Baeva et al [11], explicitly links the sharp variation of γ to the production of harmonics of the highest order. The new model dubbed the γ-spike model or Baeva–Gordienko–Pukhov theory (BGP) requires an, as of yet unproved, assumption which extends the theory of electric field boundary conditions at a perfect mirror. Starting with result from classical electrodynamics [12] where a reflected wave is subject to a phase shift of π giving rise to the equality

$$E_y^i(x_0, t) = E_y^r(x_0, t), \tag{5}$$

where E_y^i and E_y^r are the y components of the incident and reflected fields respectively. Moving to the oscillatory model the position of the mirror in the rest frame x_0 is replaced with $x_{arp}(t)$ i.e. the apparent reflection point (ARP). Now the equation (5) transforms into

$$E_y^i(x_{arp}(t), t) = E_y^r(x_{arp}(t), t). \tag{6}$$

Utilising the boundary condition in (6) the theory finds that since the emission of highest harmonics is restricted to a period of time much shorter than the optical period of the driving field. This emission interval T_{spike} is essentially the width of the γ-spike. As the width of the γ-spike decreases, and v_{max} increases, the degree of temporal confinement of the harmonics increases such that,

$$T_{spike} \propto \frac{T_0}{\gamma_{max}}. \tag{7}$$

Where $T_0 = 2\pi/\omega_0$ is the period of the driving field. Recalling the simple moving mirror model and supposing T_{spike} is the duration of the emitted harmonic pulse we can deduce that the pulses are compressed by a factor of $4\gamma_{max}^2$.As a result the temporally narrow bunches of radiation will be emitted with a duration,

$$T_{bunch} \propto \frac{T_{spike}}{\gamma_{max}^2} \propto \frac{T_0}{\gamma_{max}^3}. \tag{8}$$

Indeed, the reflected radiation will contain sharp changes in field strength (demonstrated in Fig. (2)) on the order of T_{bunch}. Therefore, by Fourier transforming the field we should find it to contain frequencies up to the order of $\omega_{max} \propto \omega_0 \gamma_{max}^3$.

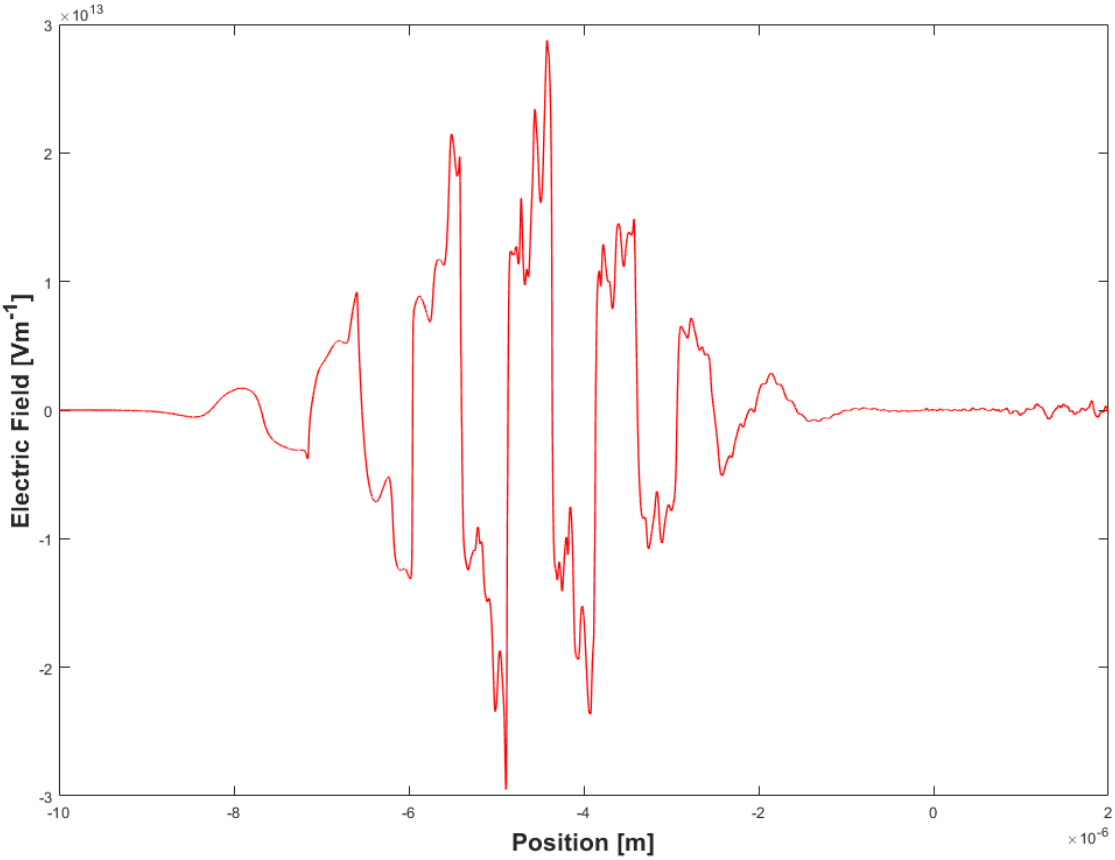

Figure 2: Electric field profile of a pulse with $\lambda = 1\mu m$ and 10fs duration, reflected from a cold quasi-neutral plasma situated between 0 and $2\mu m$. Note the sharp transitions visible at the peaks due to high harmonics. Oscillations on the far right of the diagram caused by imbalances in the charge density in the plasma following the interaction.

As is the case with many theories, the model is not without flaw [13]. The main limitation of the γ-spike theory derives from the base assumption given in Eq. (6) as the relation is not strictly correct. Figure (3) illustrates the intensity mismatch between the two fields following an interaction resulting in HHG. The substantially different intensities result from electromagnetic energy being concentrated in a short interval for each laser cycle. Regardless of the motion of the ARP, equation (6) does not hold for all times when $|E^r| > |E^i_{max}|$.

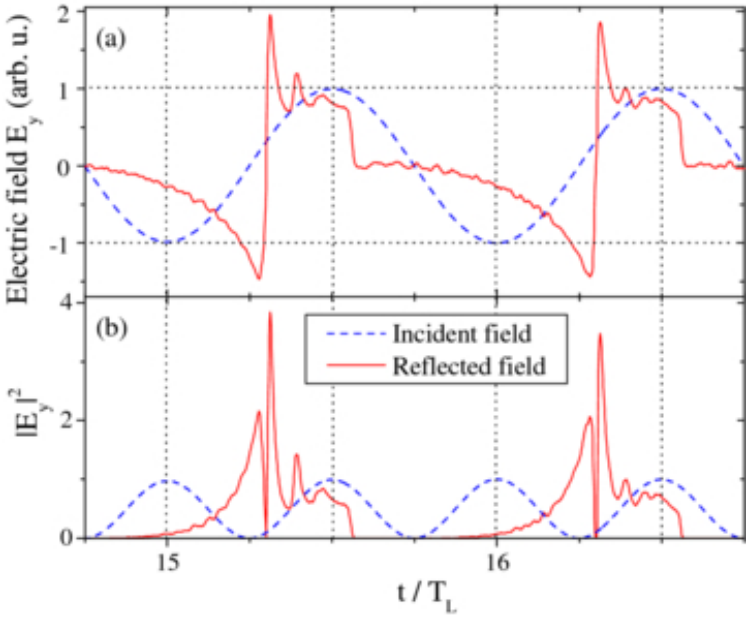

Figure 3: (a) Comparison of field intensity prior to and after interaction with the plasma. (b) Magnitude of the electric fields $|E_y|^2$ proportional to the energy density in the pulse clearly displays the redistribution of energy in each cycle. Reproduced from [14].

3.2 Atto-second Pulses

While the reflected field contains pairs of high harmonic bunches per cycle, we must remember that this radiation is riding atop the driving field. In reality the spectral intensity of ω_0 is simply overwhelming compared to the harmonics as explained by the extended theory [10, 11] of the ROM which predicts the harmonic conversion efficiency η as a function of the harmonic order so that

$$\eta(n) \sim n^{-8/3} \tag{9}$$

with n being the harmonic order. Hence, in order to fully utilise the generation mechanism steps must be taken to ensure the removal of low frequency radiation. Experimentally this may be achieved through the application of a physical filter such as Aluminium (in Fig.4), chosen specifically for high transmission at the relevant frequencies.

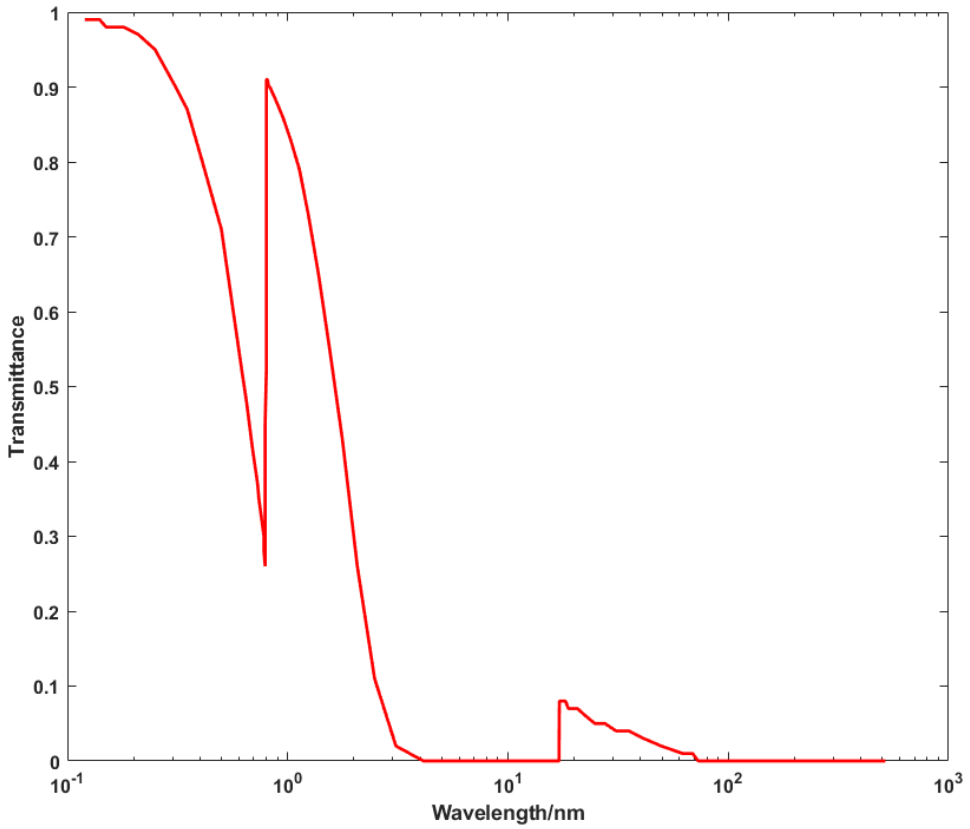

Figure 4: Transmittance of Aluminium as a function of wavelength between $0.12nm$ and $516nm$. Data demonstrates elevated transmittance below $\sim 10nm$ with a dip to $< 30\%$ transmittance around $\sim 1nm$. Generated using data from Ref. [15].

Minimising the intensity of the fundamental field via a high-pass filter facilitates the extraction of pulses with the shortest temporal duration. The magnitude of the atto-second pulse duration is in large controlled by the dominant frequency in the pulse and its bandwidth. It follows that great care must be taken into choosing a wide enough filter so as to not diminish the overall conversion efficiency. High-pass filters with a narrow permissible bandwidth will only result in pulses of negligible energy compared to harmonics of lower order. In fact studies into realistic filters and intensities produced by modern lasers suggest that acceptable performance may be possible, with one particular study finding the efficiency of a $84as$ pulse centred around $20 - 70eV$ to reach a few percent of the incident field intensity [16].

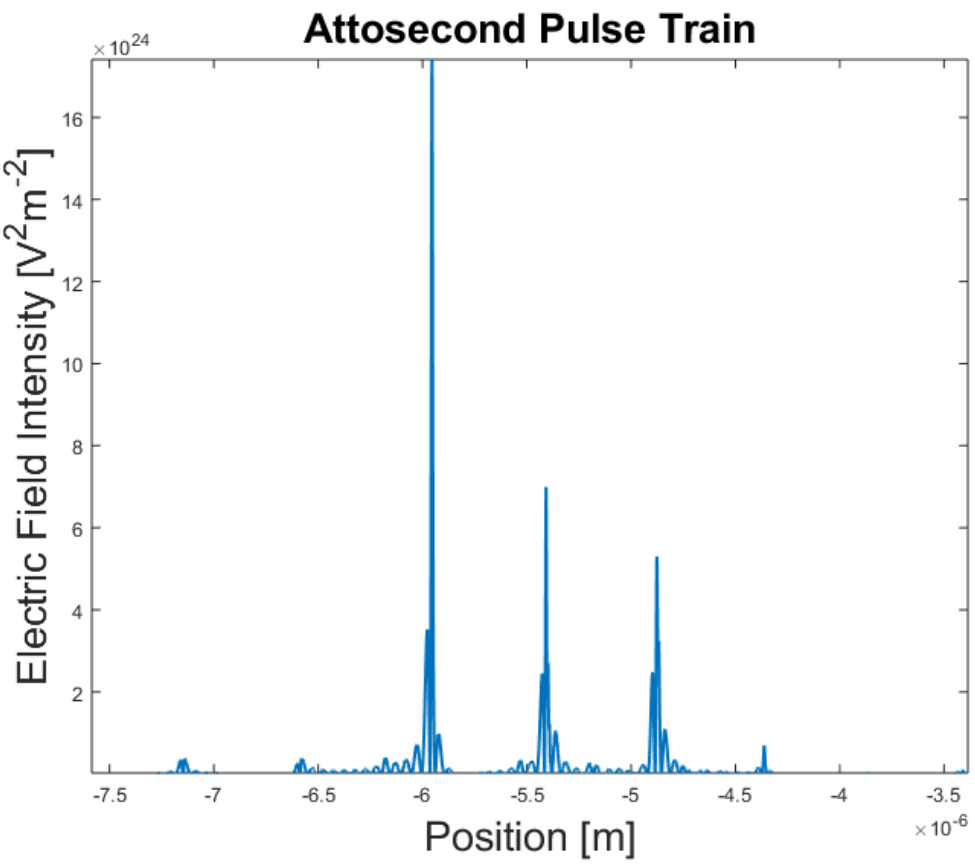

Figure 5: Atto-second pulse train following filtering such that harmonics below $n \sim 10$ effectively removed from the spectrum. Results obtained from 1D particle-in-cell simulation with normally incident pulse where $\lambda = 1\mu m$ and $\tau_0 = 10fs$ (FWHM).

3.3 Pulse Gating

Evidently the next step after producing trains of atto-second pulses would be the reliable and efficient production of individual atto-second pulses or IAPs. Here one apparent method of temporal restriction involves exercising control over the carrier envelope of the pulse by minimising the pulse duration τ_0 relative to the central wavelength of the pulse λ_0 thereby reducing the number of half cycles contributing to the HHG pulse train, with the ideal case of the envelope wide enough to admit a single cycle. This particular method of rapidly varying the field intensity so as to produce a single cycle pulse is known as intensity gating.

Intensity gating has already been implemented by controlling the phase of the wave in relation to the peak of the envelope. Tailoring this carrier envelope phase (or CEP) has been shown to maximise harmonic generation down to a single cycle in experiments using the gas harmonic generation mechanism. The work by Goulielmakis et al. [7] relied on fine-tuning the near-IR peak intensity to achieve the widest possible EUV spectrum and thus the shortest pulse duration, which ultimately

facilitated the creation and measurement of a single $\sim$ 80as pulse, very close to the transform limit of 75as.

One competing gating method known as polarisation gating, is possible due to the inherent sensitivity of the harmonic generation mechanism in gases to the polarisation state of the incident light [17]. For increasing degrees of ellipticity in the incident laser field the efficiency of harmonic generation was found to decrease for the highest harmonics, with the low order harmonics being less affected by ellipticity. Exploiting this property of the polarisation state, Corkum et al [18] combined two short laser pulses, with the polarisation of each pulse being offset by 90° with respect to the other. The experimental setup usable for polarisation gating is presented in figure (6). The wavelengths of the two pulses were chosen specifically such that,

$$\frac{\omega_1 - \omega_2}{\omega_1} << 1. \tag{10}$$

This results in a pulse with a polarisation which begins as circular and varies into linear at the peak of the pulse followed by circular polarisation at the trailing edge of the pulse. Controlling the overlap between the two pulses and their respective wavelength allowed the width of the linearly polarised section of the pulse to contained down to a single half cycle of the driving field.

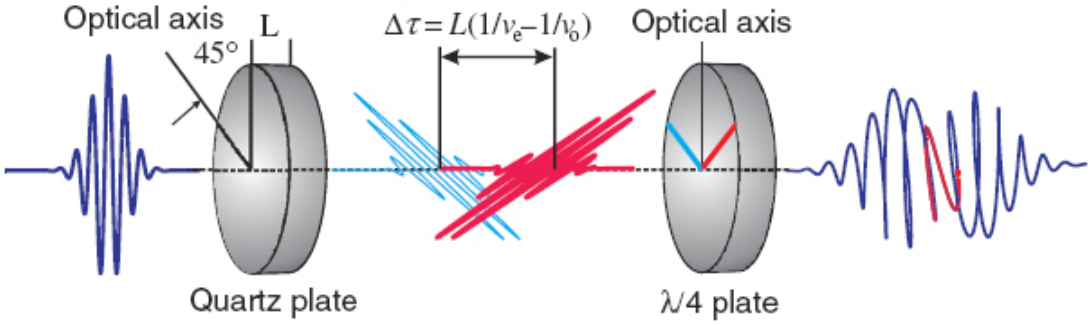

Figure 6: Schematic of proposed polarisation gating experiment. The first birefringent plate splits the incident linearly polarised pulse into a pair of pulses with a short delay Δt, polarised at right angles with respect to each other. A quarter wave plate placed further down the beam line with an optical axis at 45° relative to both components, alters the polarisation from linear to circular with a short interval on the order of Δt where the polarisation is linear. Reproduced from [19].

Similar results have been demonstrated using particle in cell simulations studying SHHG [19, 20], in theory allowing the schemes to extend to the SHHG regime.

4 Non-collinear optical gating

4.1 NOG basic concepts

The gating methods discussed thus far, in one way or another rely on the temporal restriction of the generating period. However, gating can be achieved through clever spatial manipulation instead. If a particular interaction produces a train of atto-second pulses, instead of gating the train to obtain a single pulse perhaps the pulses could be separated to yield multiple usable atto-second pulses. If

each atto-second pulse obtains its own unique propagation direction, conventional optical devices such as mirrors and lenses could be used to fully isolate each signal.

Previous experiments and theory have in the past demonstrated the relation between the emission direction of the harmonic radiation and the instantaneous direction of the wave-fronts of the driving field. For gas harmonics this is the propagation direction in the gaseous medium, while in the case of SHHG this is parallel to the wave-vector $\mathbf{k}$ of the reflected field (fig. 7). In principle if one were to achieve a rotation of wave-fronts either in the medium or at the plasma-vacuum boundary the direction of emitted harmonics will vary correspondingly.

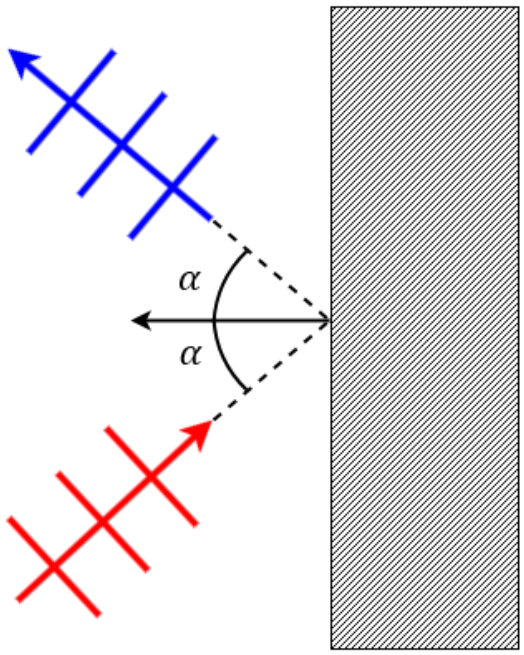

Figure 7: Direction of emitted harmonics follows the law of reflection which requires the angle of incidence to be identical to the angle of reflection. On a deeper level, the emission direction is linked to the wave-front direction at the vacuum-plasma boundary. This picture becomes more complex given a continuous boundary with the vacuum.

One gating method producing wave-front rotation has been proposed for HHG in gases by Heyl et al [21] and demonstrated experimentally by Louisy et al [22]. The method known as non-collinear optical gating or NOG requires two short laser being focused non-collinearly into the gaseous generation medium. Here non-collinear refers to each of the pulses possessing a unique propagation direction but travelling in the same plane at the focus. At focus, the propagation vectors $\hat{\mathbf{k}}_1$ and $\hat{\mathbf{k}}_2$ form a sector of angle 2α. Furthermore the pulses are offset in time by a short delay Δt such that the interval between the arrival of the pulses is Δt. Harmonic generation in this geometry creates angularly separated pulses at the bisector of the driving lasers, essentially separated from the fundamental field. In the case of ideal gating a spatial filter would be all that is

necessary to remove the driving field which may be orders of magnitude greater than the produced high frequency harmonics. The geometry is illustrated in Figure (8).

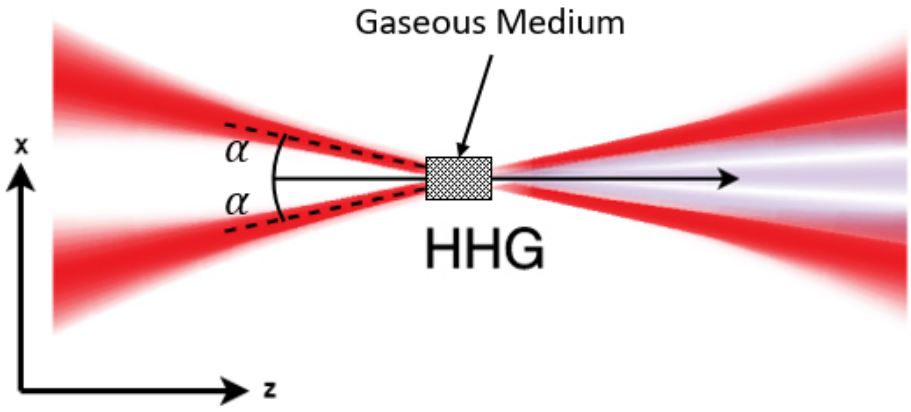

Figure 8: Basic diagram of the NOG geometry used in gas HHG. The generation medium is typically a gas filled cell or a jet of gas. Partially reproduced from [21].

The wave-front rotation in this generation scheme arises due to the changing amplitude of the two pulses as they pass the focus. As the first pulse arrives the wave-fronts of the generated harmonics are aligned with the first pulse and propagate along $\hat{\mathbf{k}}_1$, however as we advance time the intensity of the second pulse increases causing the wave-front at the focus and harmonic propagation direction $\hat{\mathbf{k}}_h$ to rotate towards $\hat{\mathbf{k}}_2$. The direction of the emitted harmonics $\hat{\mathbf{k}}_h$ due to the fields at the point of intersection can be expressed as

$$\mathbf{k}_h = \frac{\mathcal{E}_1(t)\mathbf{k}_1 + \mathcal{E}_2(t)\mathbf{k}_2}{\sqrt{\mathcal{E}(t)_1^2 + \mathcal{E}(t)_2^2}}. \tag{11}$$

In the above relation $\mathcal{E}_{1,2}(t)$ represents the amplitude of each pulse envelope as a function of time. For Gaussian laser pulses this envelope function is given by

$$\mathcal{E}_{1,2}(t) = \exp\left[-2\ln 2\frac{(t \pm \Delta t/2)}{\tau^2}\right]. \tag{12}$$

In the above relation τ is the pulse duration i.e. FWHM, while the $\Delta t/2$ term is due to the relative delay in time being Δt. Using the result of equation (11) we can obtain the angle of emission relative to the z-axis by taking the scalar product with the x-axis such that $\mathbf{k}_h \cdot \hat{\mathbf{x}} = -\sin\beta$ where β is the angle of interest. Taking this derivation further, Heyl found that for small angles α, the angle β is approximated by

$$\beta = \alpha \frac{1-\xi}{1+\xi}. \tag{13}$$

This result explicitly relates the ratio of the field amplitudes $\xi = \frac{\mathcal{E}_2}{\mathcal{E}_1}$ to the wave-front rotation at focus. Now, by introducing the delay between pulses Δt on the order of the laser period T, the amplitude ratio changes rapidly from one cycle to the next. As a result the change in the propagation angle β will occur on the timescale of Δt and the relation $\Delta t \approx T$ is known as the ideal gating condition. Harmonic radiation emitted during this period will be angularly streaked as the wave-front direction will be different for each half cycle. For delays where $\Delta t >> T$ the pulses see no temporal overlap and the radiation is emitted at $\pm\alpha$. Conversely if there is no delay between pulses the emission will take place parallel to the z-axis as the x-components of each field cancel out.

4.2 Comparison with the Atto-second Lighthouse

The NOG technique is conceptually similar to a different technique known as the atto-second light house which relies on wave-front rotation to produce streaked atto-second pulses. The effect utilises pulses with an applied angular chirp which results in each wave-front in the pulse pointing in a different direction. As the wave-fronts arrive at the generation medium each wave-front creates an individual atto-second pulse with a unique direction.

The pulses used by the ALH scheme are angularly chirped, that is the pulse is chirped across its beam profile, perpendicular to the propagation direction as demonstrated in Figure (9).

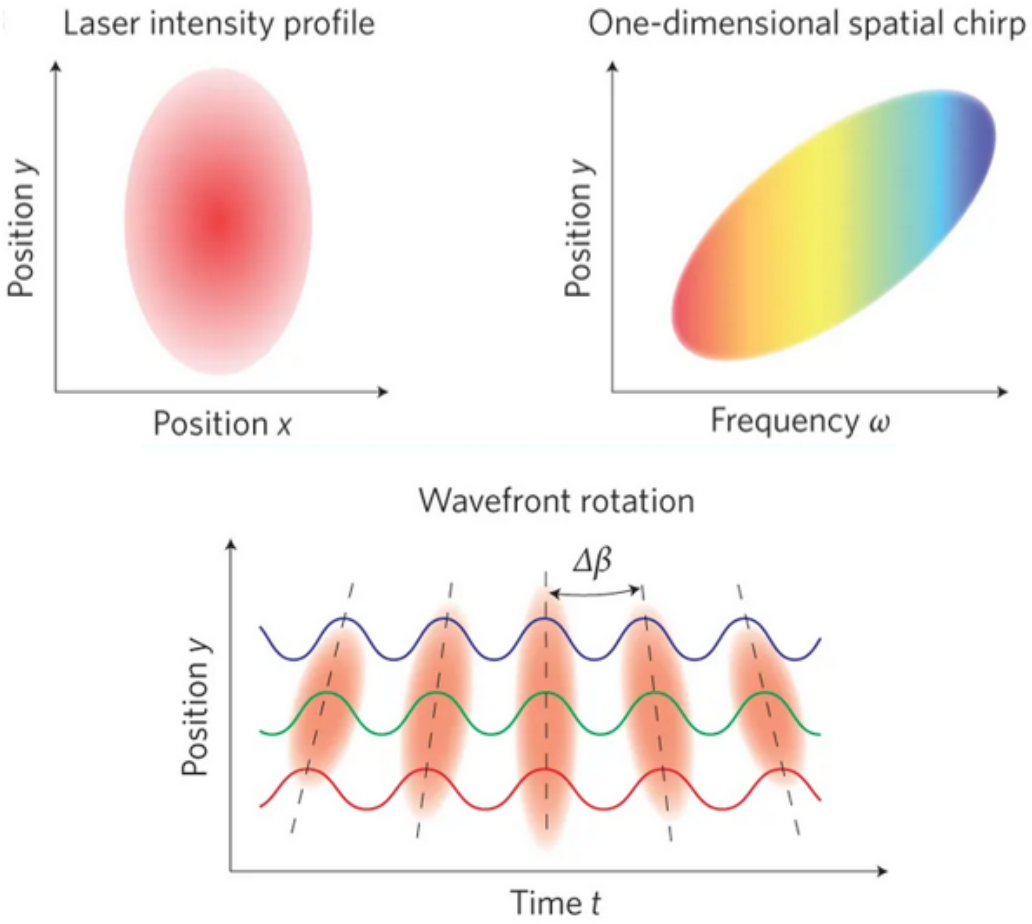

Figure 9: The wave-front rotation can be achieved by dispersing the wavelengths of a broadband pulse along a single direction at focus. Partially reproduced from [23].

At present little to no effort has been spent on implementing the NOG technique for use with the SHHG mechanism. Taking advantage of the wave-front rotation in a SHHG setup has been implemented in the past using the atto-second lighthouse technique [23], as such there is little in the theory which should forbid the NOG geometry from being utilised as well. The obvious advantage of NOG over the ALH scheme is the simple experimental implementation requiring only two femto-second pulses which are readily available with modern tabletop laser systems. Additionally filtering of reflected radiation becomes simpler using NOG as the harmonic radiation is separated from the fundamental field. Depending on the degree of separation, judged by the total intensity of the first harmonic ω_0 in the spectrum of one of the streaked pulses. Total separation from the fundamental is of course unlikely since the laser pressure will deform the plasma surface thereby leading to focusing and altered divergence of the driving field. In contrast, the pulses created by the ALH

lie within the angular range of the driving field. Theory [21] suggests that the maximum rate of wave-front for NOG is higher than for ALH. The benefit here is explained as a larger divergence between each consecutive atto-second pulse. Of course since no experimental investigation has been carried out for the mechanism for plasma surfaces all of the given advantages remain as little more than conjecture at present.

5 Laser-plasma simulations

The preliminary work in implementing the NOG geometry in plasma must rely on performing simulations using PIC codes to gain an insight of what the expected experimental results may look like in the future. The simulations are therefore an inexpensive manner of probing the technique and letting us glance at the potential experimental considerations which must be taken into account in a real experiment. This section will aim to give an overview of the particle in cell method of simulating plasma and discuss a few of the downsides associated with computational modelling of interactions such as SHHG. Finally the computational implementation of NOG will be described in detail for SHHG.

5.1 Particle-in-cell codes

The simulations described in the later parts of the report are based entirely on particle-in-cell codes. These are computational models used to probe the evolution of a system of charged and neutral particles under the influence of a field by simulating collections of particles scattered within a grid of cells. The codes often approximate large numbers of individual particles as a smaller set of heavier "macro-particles". This trick of using macro-particles is a way of boosting computational efficiency as simulating every single particle in an interaction is often not feasible, thus requiring us to re-scale the number of particles via the use of macro-particles. Each macro-particle represents a collection of real particles and possesses a mass and charge equal to a sum over all individual constituent particles.

Once defined, the macro particles are moved by an algorithm called the particle pusher in accordance with the equations of motion and the Lorentz force:

$$\frac{d\mathbf{r}}{dt} = \frac{\mathbf{p}}{\gamma m} \tag{14}$$

$$\frac{d\mathbf{p}}{dt} = \frac{q(\mathbf{E} + \mathbf{v} \times \mathbf{B})}{\gamma m} \tag{15}$$

The quantities $\mathbf{p}$, $\mathbf{r}$, m, γ are , momentum, position, Lorentz factor and mass, respectively. The fields behind the motion here are the electric field $\mathbf{E}$ and the magnetic field $\mathbf{B}$.

The specific PIC code used in the preparation of this report called EPOCH relies on the Finite-difference time-domain method or Yee's method used for modelling computational electrodynamics. The implementation depends on defining a grid of points known as a computational domain. The fields $\mathbf{E}$ and $\mathbf{B}$ are then defined at each point in this space. Additionally each each point in space must be associated with a permittivity and permeability unique to a particular material whether it be vacuum, a dielectric or a conductor. Finally the sources of fields are mapped onto the grid and field is allowed to evolve in time through solving Maxwell's equations:

$$\frac{\partial \mathbf{B}}{\partial t} = -\nabla \times \mathbf{E} \tag{16}$$

$$\frac{\partial \mathbf{E}}{\partial t} = \nabla^2 \times \mathbf{B} - \epsilon_0 \mu_0 \mathbf{J}. \tag{17}$$

To be of any use computationally the equations must be made discrete by replacing the field derivatives with finite differences:

$$\frac{\partial}{\partial t} f(x,t) \rightarrow \frac{\Delta f(x,t)}{\Delta t} \tag{18}$$

$$\frac{\partial}{\partial x} f(x,t) \rightarrow \frac{\Delta f(x,t)}{\Delta x} \tag{19}$$

The, now discrete, Maxwell's equations are then solved to obtain "update" equations which express the future fields in terms of past fields. The electric and magnetic fields are then evaluated using the update equations at the next simulation time-step. The resulting, new fields are fed to the particle pusher which uses the discrete versions of equations (14) and (15) to update the new positions and velocities of all macro-particles. The loop starts again by using the new particle positions and velocities to define the new currents and charge densities for the next time-step. This process is repeated until a desired field state is achieved or until enough data about the system being modelled has been collected.

5.2 Simulation Considerations

Before going on to model the SHHG in the NOG geometry it is worthwhile taking note of certain crucial simulation parameters and how they will affect the simulation. The first important parameter being the spatial resolution of the simulation. Here the resolution refers to the physical dimensions of cells on the grid. We require that the spatial resolution in any given simulation must as fine so as to resolve the interaction of interest. As the field is necessarily defined and sampled for output at each grid-point, the finer changes in the field during an interaction will be lost. It is especially important, when simulating a plasma that the grid is sufficiently small so as to resolve the plasma frequency. A sufficiently dense quasi-neutral plasma will be effectively collision-less and most of the electrodynamic properties can be inferred directly from the plasma frequency itself. Not being able to resolve the plasma frequency implies we also cannot resolve main physical processes within this plasma, nor can we resolve any changes in the field with a wavelength smaller than the grid.

Linked closely to the spatial is of course the temporal resolution defined as the time-step of each iteration. Depending on the specific integration scheme used to evolve the simulation forwards in time, there exists a relation between the minimum spatial resolution and the smallest necessary time-step. This relation is generally known as the Courant–Friedrichs–Lewy or CFL-condition:

$$\frac{c\Delta t}{\Delta x} + \frac{c\Delta t}{\Delta y} \leq C_{max} \tag{20}$$

Δt, Δx, and Δy define the time-step and grid dimensions. The constant C_{max} is the Courant number and depends on the nature of the discretisation scheme. In the case of the FTDT scheme employed by EPOCH, the default value of 0.95 is applied.

Obviously one should aim to choose the maximum possible time-step which still allows us to resolve the physics of interest while preserving the accuracy of the simulation at an acceptable level. The unfortunate consequence of using discrete equations of motions as opposed to their continuous counterparts, is the introduction of numerical errors which accumulate over the course of a simulation, skewing results by either over or underestimating values with each successive time-step. On the other hand decreasing the time-step prevents the accumulation of errors at the cost of the increased computational overhead.

Unlike an experiment, the simulation is severely limited by the maximum size of the domain. In short, the domain has bounds. In time this boundary is the duration for which it runs, in space however this is the size of the grid. In time the boundary is simple; a simple flag marking the stop-time will suffice. In space this is not as simple. For that reason EPOCH allows the user to tailor the simulation's edge to suit their needs by supporting a few different types of boundaries.

Open boundaries are often used to simulate empty space outside the simulation. These boundaries allow particles and fields to pass through, hence effectively leaving the simulation. Due to this open boundaries will in certain cases decrease the simulation workload as fewer and fewer particles need to be simulated. While useful in many settings the downside of open boundaries for fields lies in how they are effectively truncated at the boundary. Waves in the electromagnetic field do not pass through the boundary smoothly but are partially reflected. A potential remedy for this is using an absorbing medium extending past the boundary. This new absorbing boundary is called a perfectly matched layer or PML. EPOCH uses a specific implementation of PML called the Convolutional Perfectly Matched Layer (CPML) method.

Boundaries can also be periodic, such that particles crossing a boundary on one side of the simulation reappear on the opposite side of the grid, conserving the total number of particles and the field energy density.Similarly this can of course be applied to fields passing a boundary.

5.3 Simulation Parameters

With the parameters and all the special considerations taken into account, we may now begin describing the final setup of the simulation including the laser and plasma geometries used. For speed EPOCH was customised to produce a 2D simulation with a square grid of 20 by 20 microns. The resolution used in the simulations ranges between 2000 cells in the x and y directions to 8000 cells in each axis. Higher resolutions were used in certain cases to obtain more accurate and detailed spectra. Additionally, the boundaries are open and set to use the CPML boundaries to minimise the noise from boundary reflections. A basic diagram of the simulation box is presented in Figure (10).

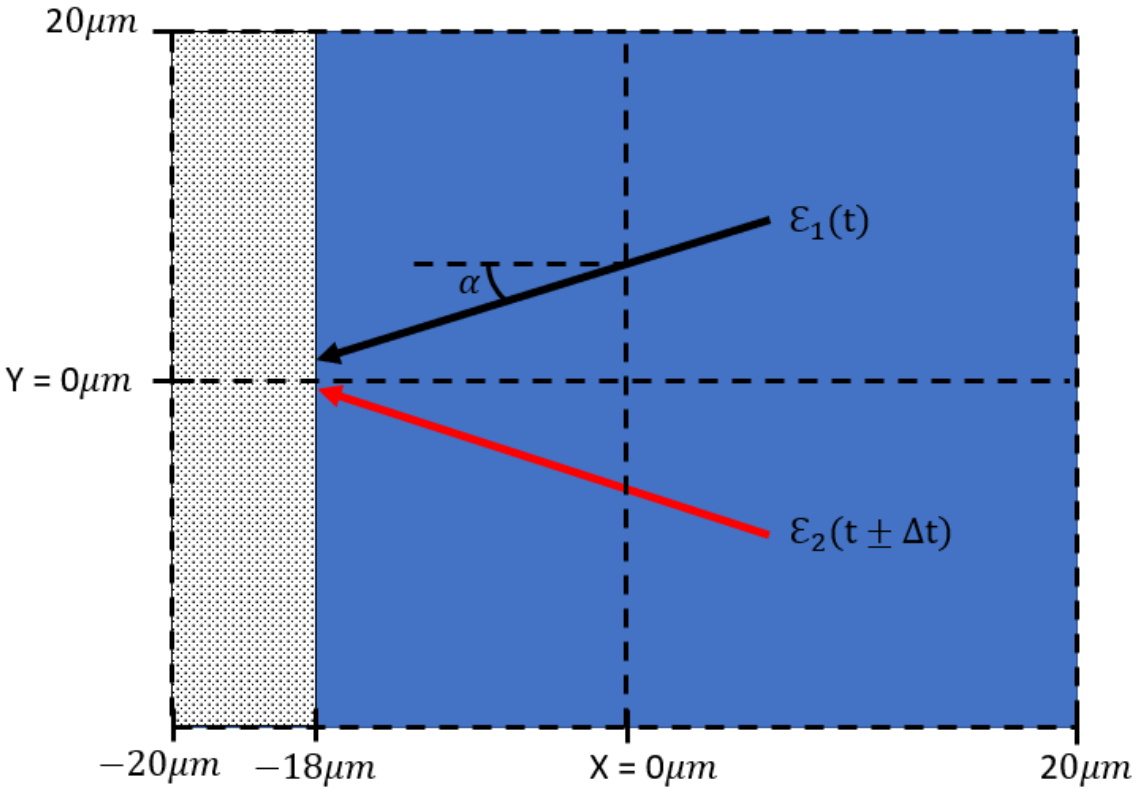

Figure 10: Simple diagram of the simulation space. The lasers represented by the red and black arrow originate from the right boundary and are focused onto a spot on the plasma surface at coordinates $-18, 0$. Diagram does not accurately portray a scale length in front of the plasma ranging up to $1\mu m$ in width. the blue space covering a large proportion of the box represents the vacuum. The plasma surface is visible on the left.

One of the most important features of the simulation are the laser sources. As with NOG in gases, the plasma surface implementation uses a pair of lasers with a time delay δt between them. The lasers originate from the right edge at $x = 20$ and travelling to the left border at $x = -20$, towards where the plasma surface lies. The wavelength of the lasers has been set as $1\mu m$ while the full angle between the lasers is $2\alpha = 1^\circ \approx 17$ mrads. The peak pulse intensity is $10^{21} W cm^{-2}$ This wavelength is potentially a good choice for investigation due its accessibility via modern lasers. Now, in order to implement the angle, the laser pair must emerge from the right boundary at different height. The specific height is calculated such that if the laser surface is moved closer, both lasers still focus in the same in the same height on the surface where $y = 0$. The envelope used was a standard Gaussian envelope with the pulse duration $\tau = 5fs$.

Positioned at the left boundary between $-20\mu m$ and $x = -18\mu m$, the plasma surface has a number density of $100n_c$ (for $\lambda = 1\mu m$) corresponding to $1 \times 10^{29} m^{-3}$ for both negative and

positive particle species. The modelled particle species posses charges and masses identical to those of the electron and proton with the number of macro particles per cell being 10. As the efficiency of the conversion mechanism is sensitive to the density gradient [24] at the plasma vacuum interface the simulation included an exponentially density ramp known as a scale length, falling off by $1/e$ over the length of a $1\mu m$. To reduce noise and dissipation of the established scale length, the temperature of the two species was set to 0K.

Following a reflection from plasma, the field is directed back towards its source at $x = 20$. At $70fs$ into the simulation the code switches to the "Window" mode provided by EPOCH allows the reflected field to propagate in the x direction for a set period of time. This allows any streaked pulses to diverge making observations easier. In this mode the program simply moves the simulation window in a specified direction at a speed set manually by the user. The other benefit of the window function is that it reduces noise due to electrons ejected from the surface by the laser field. Since electrons cannot travel at the speed of light, they are left far behind after propagating the waves for a few hundred femto-seconds. After the propagation the window function is turned off and the simulation box is stationary again. The field can now be be sampled as a function of time along a vertical line at $x = 0$ and ranging from $y = -20\mu m$ to $y = -20\mu m$. The following sampling interval goes on for a total of 50fs which allows the entire pulse to pass the sampling plane.

6 Results and Discussion

Once collected, the simulation data is processed mainly using Matlab code to perform a discrete Fourier transform and obtain the spectrum at every height on the y-axis. The first simulation run used $380fs$ for the propagation time during the window mode for a total simulation time of $500fs$. By the end of the simulation this results in the pulse diverging over a distance of $112\mu m$. From the spectrum seen in Figure (11) of the first run a few points can be made about its general shape.

First, as expected the highest intensity occurs at the first harmonic corresponding to a wavelength of $1\mu m$ with the intensity being split into roughly three peaks. The two outer peaks (i.e. off the optical axis $y = 0$) at the first harmonic can be attributed to the two incident laser pulses striking the surface and propagating at the angle of reflection. Further, there exists a substantial intensity of the driving field on the optical axis which can be explained by considering the instant the laser field envelopes are equal in intensity $\mathcal{E}_1 = \mathcal{E}_2$. The wave-front orientation at this time should be in parallel with the plasma surface. This can be explained through noting the y components of the electric field being equal and opposite in value at this time.

While the intensity of the first harmonic was split into three almost equal parts, from the 2^{nd} onward the situation begins to look different. Apart from the 2^{nd} harmonic around $y = 0$ the sharpness of each harmonic is severely reduced. The decay of harmonics quickens towards the edge of the simulation. In the centre, harmonics up to the 25^{th} are clearly visible, however at angles corresponding to the driving field the harmonics become faint and invisible at this contrast level, between the 10^{th} and 15^{th}. The generation is clearly more efficient close to the optical axis, most likely due to the high field on the surface during the short interval when the field envelopes are equal.

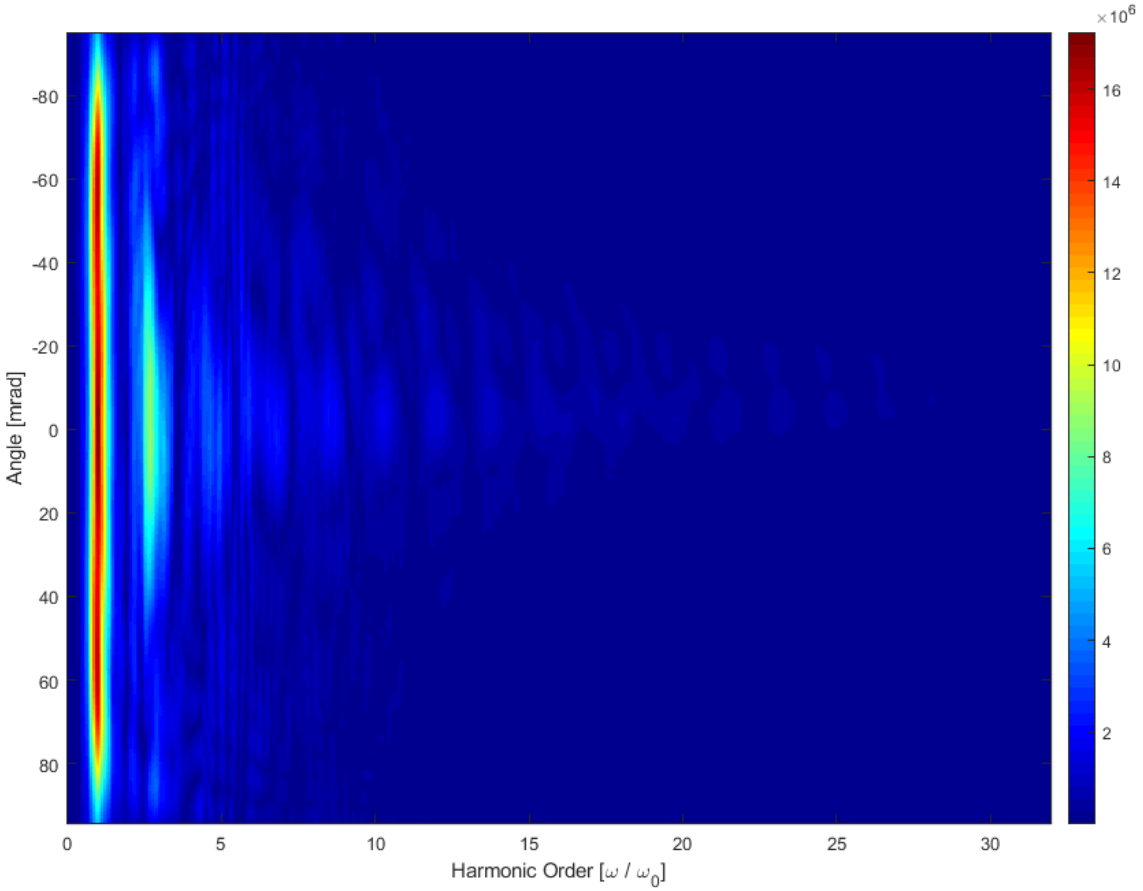

Figure 11: Spectrum from the $8k \times 8k$ cell run using the NOG geometry. Note the wide divergence of lower order harmonics and compare to the highly localised higher orders. Angle computed from the approximate distance travelled $\theta = tan^{-1}(y/112\mu m)$.

Moving past the 15^{th} harmonic, there appears to be a spatial/angular splitting into two close bands in frequency space which consist of primarily odd harmonics. The first and strongest band of harmonics propagates almost parallel to the central axis ($y = 0$ or 0 mrads) but is shifted towards -7 mrads at the highest harmonics. Meanwhile the second band is spread between -10 mrads and -20 mrads. Upon closer inspection (see fig. 12) however it does appear that there is a third distinct band of harmonics situated between 0 and 15 mrads. Comparatively weaker than the Central and off-axis bands, hence harder to spot, this band bears a great resemblance to the others due to the ordered structure of odd harmonics. Signs of other weak bands appear, however their existence only becomes more prominent at higher frequencies where noise begins to dominate.

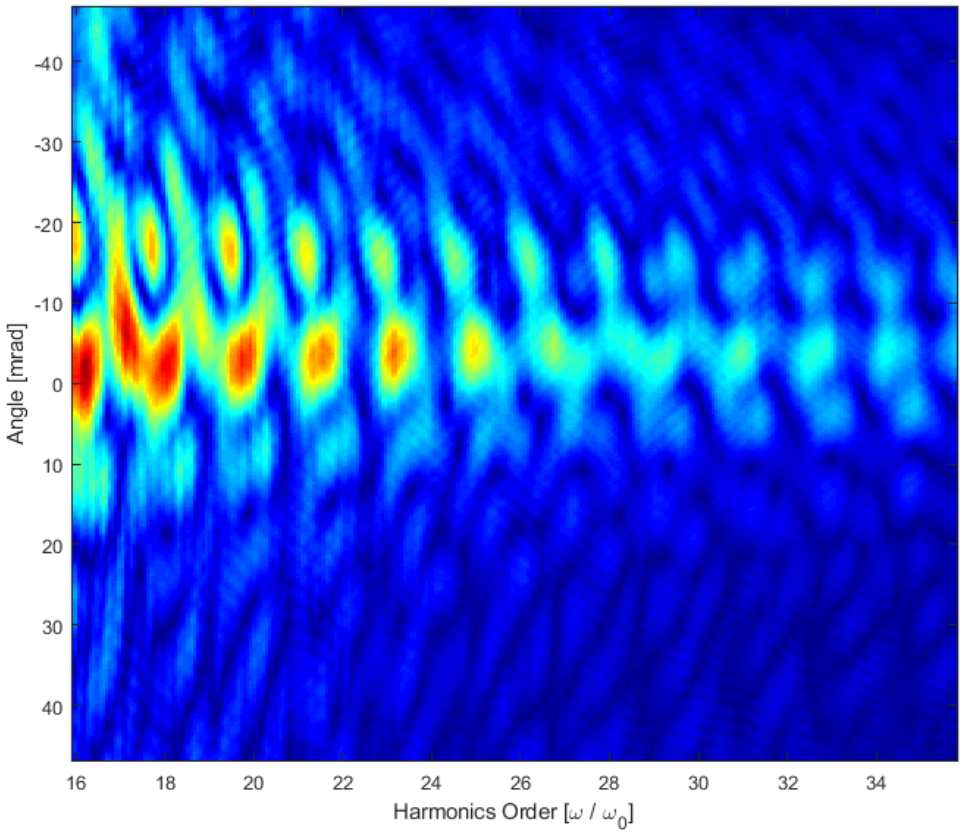

Figure 12: High contrast image of the spectrum between the 16^{th} and 34^{th} harmonic shows three bands. The central and upper bands dominate but third is clearly visible yet diffuse.

Thus far the interpretation of the spectrum for the $5fs$ pulses suggests that the interaction led to the creation of three pulse train of varying intensity. Here we may note the asymmetry of the spectrum. Centred about the strongest, middle band, the harmonics appear to be shifted in the direction of the first incident pulse. It therefore becomes a reasonable assumption that the incident pulses are the origin of the three main bands. Especially, noting the incidence angle of the pulses of 17 mrads which lies in the range of the upper band. Hence, it is possible the initial laser may have generated the upper band, and similarly the delayed pulse would created the weakest band in the spectrum. One might suppose the interaction with the first laser disturbed the plasma enough to decrease the generation efficiency of the delayed pulse. In fact, interchanging the pulse delay has the effect of mirroring the spectrum about $y = 0$. This adds further evidence directly linking the incident fields and the two bands.

While distinct, the two bands might still overlap, hiding other features of the spectrum. For this a further second simulation, almost identical to the first was performed. In this simulation the

pulse had been allowed to propagate for a further $500fs$, giving a total simulation time of $1000fs$ and an approximate distance travelled of $> 200\mu m$. Illustrated in Figure (13) the spectrum has widened enough to allow for full separation of the two strongest bands and confirming their angular separation.

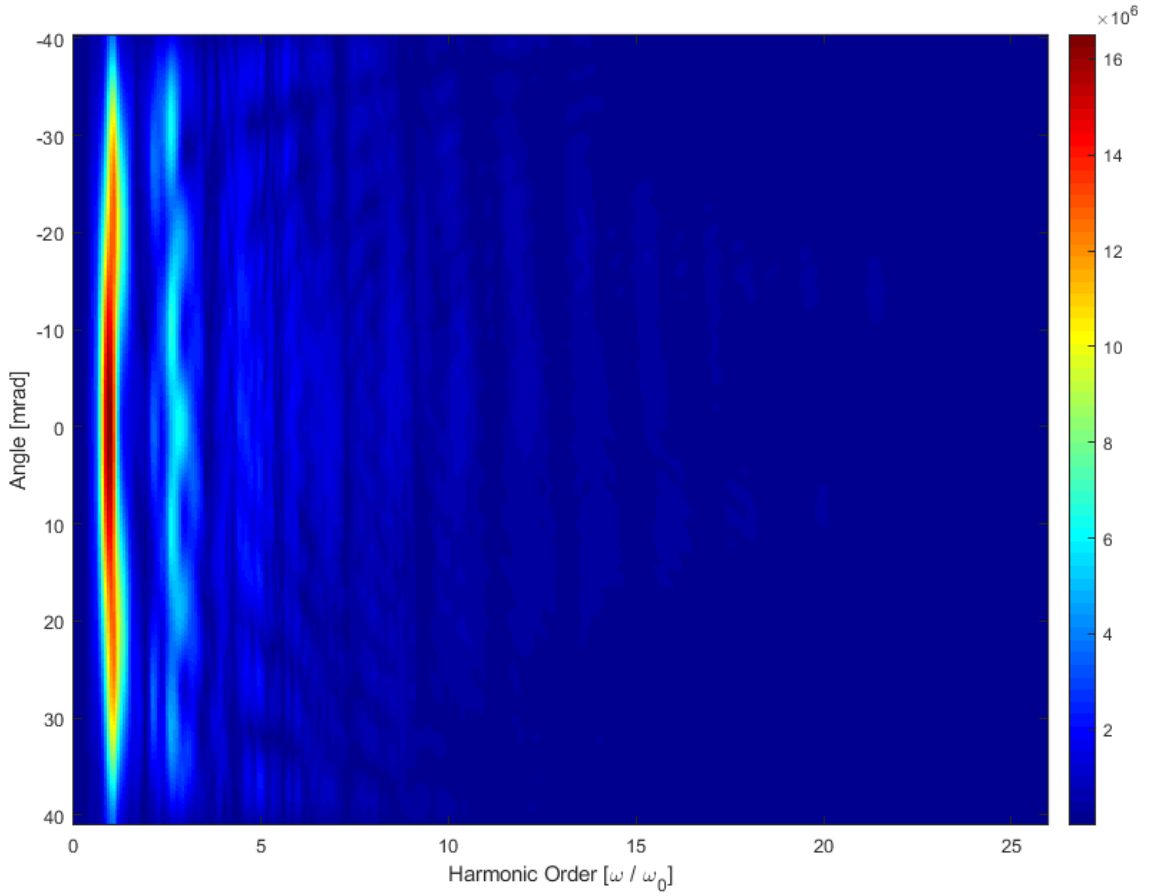

Figure 13: Spectrum after further propagation of the reflected fields. Low harmonic orders form diffuse vertical bands in the diagram with small scale features mainly attributed to noise due to the relatively low resolution used to save time. Increasing in order, the bands converge forming spatially separated spectra. Resolution of the simulation $5k \times 5k$ is likely responsible for the lack of strong harmonics in the range $20 - 25$.

With the previous assumption regarding the central band having been formed due to the combined action of the driving fields. Furthermore, we can attribute the small shift off centre as being caused by the lasting effect the primary laser on the plasma.

As the intensity of the delayed pulse increases, the plasma will respond however the deformation has already occurred. If for instance the delayed pulse had encountered the initial, flat plasma surface, the picture might have been different. This proposition could potentially be tested in

future simulation by increasing the plasma density. With a higher density the deformation or plasma denting is expected to reduce as the plasma can respond quicker to locally applied fields without suffering more global deformation.

6.1 Effect of surface denting

In the time domain, the influence of the denting phenomenon is easier to visualise and describe as are the spatially separated pulses. In Figure (14), the field exhibits previously seen asymmetry favouring initial pulse. There are also individual regions of intensity, appearing as trains of short pulses. Again, as expected, three distinct pulse trains can be identified propagating at angles commensurate to the bands seen on the spectrum. A curious point to note is the tendency of the pulses to move towards the optical axis with time. The effect is strongest for the first few pulses which quickly begin to converge towards the optical axis, though this change in direction becomes less pronounced as time passes. Specifically, for the upper pulse, situated between -10 and -20 mrads, at $t = 467fs$ each subsequent pulse shifts at an approximate rate of 2 mrads/fs until around $t = 472$ when the rate decreases to a minimum of 0.5 mrads/fs.

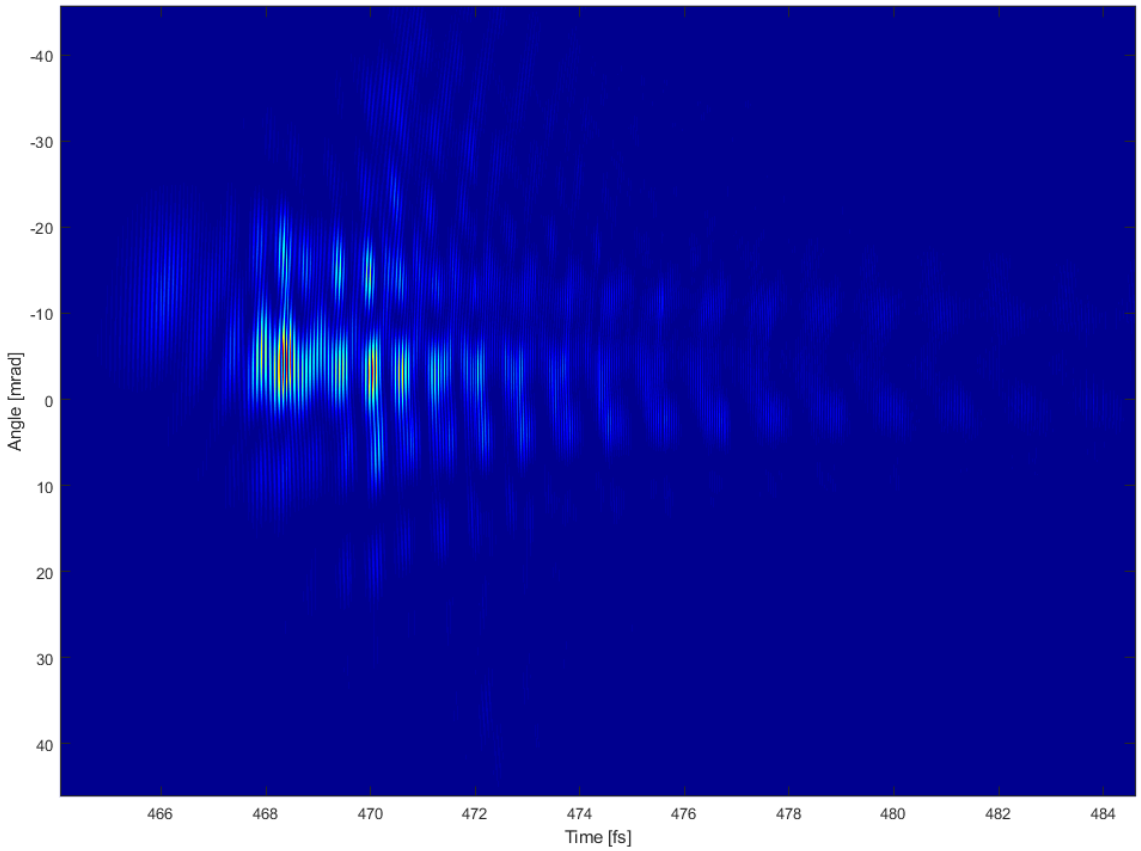

Figure 14: Magnetic field intensity as a function of angle and arrival time at the measuring plane. Obtained by filtering the spectrum of the 8k run to remove frequencies lower than the 20^{th} harmonic. Majority of the intensity directed between $\theta = 0$ and $\theta = -20$ mrads.

We should recognise the wave-front orientation physically disturbing the plasma via the pondero-motive force. The laser forces and maintains the wave-front orientation and hence the plasma surface while the pondero-motive force acts to push charges orthogonal to the wave-vector of the laser. The result is a dented surface which typically affects the reflection of the incident beam. Experimentally [25], this effect is substantial at high intensity and may lead to beam focusing. From these findings it would be acceptable to suggest that it is in fact the surface denting which is responsible for the angle varying in time. It is the fault of the surface deforming while the reflection is in process. Of course this deformation is still small and on scale of the wavelength of the fundamental it is essentially negligible, causing the lowest harmonics to spread out in a wide cone bounded by the two fields. The highest harmonics however see a curved surface, akin to a parabolic mirror which focuses the radiation into a tight angular range.

Certainly these are streaked atto-second pulses, since their direction varies, however whether this is due to the NOG geometry or simply plasma denting is unclear. So far the evidence, suggests the streaking to be caused by denting of the plasma surface which in turn focuses the two reflected

harmonic beams and the central towards the optical axis. Certainly a focus should be placed on investigating the effects of the variables: the carrier envelope phase of both pulses, the pulse length τ, the time interval between the arrival of the two pulses Δt, and in order to minimise the effect of plasma surface denting higher plasma densities should be utilised.

Clearly, NOG in gasses and off plasma not only in the choice of medium but in the interaction itself. In gases the physical behaviour of the gas as it is distorted by the laser pressure has minimal effect on the resulting radiation. Not to mention that the medium is almost perfectly transparent while the plasma is opaque and reflective. Not only does the instantaneous wave-front orientation matter in the process but the actual behaviour of the plasma density at the moment of the reflection.

To better understand the interaction, a potential direction in future research would focus on the shape of the plasma surface foll lowing reflection. As mentioned previously this will leave a dent or hole in the surface, the shape of which could be approximated as circular. Using classical optics, the foci for the incident off axis beams can be estimated providing the first steps in developing a model of reflected radiation using NOG. A model which takes into account the surface denting and tests the feasibility of NOG for low plasma densities susceptible to denting.

7 Conclusion

In summary, the report touches on the intricacies of laser-plasma interactions with a heavy focus on simulating the high harmonic generation mechanism from plasma surfaces. In theory able to unlock the yet unharnessed intensities far above $10^{21} W cm^{-2}$ available today. One potential research avenue known as Non-collinear Optical Gating has been briefly explored in the context of HHG from plasma surfaces rather than gasses as originally planned by the schemes creators.

The NOG scheme predicts a series of angularly separated pulses, with each pulse travelling in a slightly different direction. This prediction is found to be less than clear in the case of plasma. Surface denting contributes to significant focusing of the reflected harmonics, with the greatest effect occurring for the lowest orders. From the spectrum of the reflected field, angular separation of harmonics is pronounced for the highest harmonics while the lower orders are dispersed almost uniformly across the angular range. The existence of angular separation however does not align with the prediction of angularly streaked pulses. Instead there exist pulse trains, which are believed to correspond to the incident fields and have been greatly focused by the denting of the plasma surface. It is worth noting that subsequent pulses in the train do exhibit a shift in propagation direction, however rather than this being, the predicted angular streaking due to wave-front rotation at the focus, the reduction of this effect over time should suggest that it is surface denting which causes the change in angle. While not concrete evidence of denting being the prime cause it is the most likely suspect in absence of any significant pulse streaking.

The absence of streaked atto-second pulses may be attributed to the denting of the surface hence making the effect harder to observe in plasma, however this may be remedied in the future by using higher a higher plasma density to mitigate the impact of surface denting. Further optimisations could also be introduced in the scheme. No investigation has been made into the CEP of the two driving pulses and whether this may be exploited to optimise the scheme. In a similar fashion, the temporal separation of the pulses could be investigated and compared to theory [21], which proposes the optimal gating condition to occur at the $\Delta \approx \tau$ interval used in the simulations.

To conclude, the evidence obtained from the simulations proves insufficient to classify the NOG scheme as an efficient method of generating single atto-second pulses. Although inconclusive, the research has highlighted possible flaws stemming mainly from poor optimisation of the simulation

parameters. Further work must be undertaken and optimisations made if the scheme is to be implemented in a laboratory setting.

References

[1] D. Strickland and G. Mourou, "Compression of amplified chirped optical pulses," *Optics Communications*, vol. 56, no. 3, pp. 219 – 221, 1985. [Online]. Available: http://www.sciencedirect.com/science/article/pii/0030401885901208

[2] S.-W. Bahk, P. Rousseau, T. Planchon, V. Chvykov, G. Kalintchenko, A. Maksimchuk, G. Mourou, and V. Yanovsky, "Generation and characterization of the highest laser intensities (10 22 w/cm 2)," *Optics letters*, vol. 29, no. 24, pp. 2837–2839, 2004.

[3] C. Haynam, P. Wegner, J. Auerbach, M. Bowers, S. Dixit, G. Erbert, G. Heestand, M. Henesian, M. Hermann, K. Jancaitis *et al.*, "National ignition facility laser performance status," *Applied optics*, vol. 46, no. 16, pp. 3276–3303, 2007.

[4] P.-M. Paul, E. Toma, P. Breger, G. Mullot, F. Auge, P. Balcou, H. Muller, and P. Agostini, "Observation of a train of attosecond pulses from high harmonic generation," *Science (New York, N.Y.)*, vol. 292, pp. 1689–92, 07 2001.

[5] P. á. Corkum and F. Krausz, "Attosecond science," *Nature physics*, vol. 3, no. 6, p. 381, 2007.

[6] P. Agostini and L. F. DiMauro, "The physics of attosecond light pulses," *Reports on progress in physics*, vol. 67, no. 6, p. 813, 2004.

[7] E. Goulielmakis, M. Schultze, M. Hofstetter, V. S. Yakovlev, J. Gagnon, M. Uiberacker, A. L. Aquila, E. Gullikson, D. T. Attwood, R. Kienberger *et al.*, "Single-cycle nonlinear optics," *Science*, vol. 320, no. 5883, pp. 1614–1617, 2008.

[8] B. Dromey, S. Kar, C. Bellei, D. C. Carroll, R. J. Clarke, J. S. Green, S. Kneip, K. Markey, S. R. Nagel, P. T. Simpson, L. Willingale, P. McKenna, D. Neely, Z. Najmudin, K. Krushelnick, P. A. Norreys, and M. Zepf, "Bright multi-kev harmonic generation from relativistically oscillating plasma surfaces," *Phys. Rev. Lett.*, vol. 99, p. 085001, Aug 2007. [Online]. Available: https://link.aps.org/doi/10.1103/PhysRevLett.99.085001

[9] A. Einstein *et al.*, "On the electrodynamics of moving bodies," *Annalen der Physik*, vol. 17, no. 891, p. 50, 1905.

[10] S. Gordienko, A. Pukhov, O. Shorokhov, and T. Baeva, "Relativistic doppler effect: Universal spectra and zeptosecond pulses," *Physical review letters*, vol. 93, no. 11, p. 115002, 2004.

[11] T. Baeva, S. Gordienko, and A. Pukhov, "Theory of high-order harmonic generation in relativistic laser interaction with overdense plasma," *Physical review E*, vol. 74, no. 4, p. 046404, 2006.

[12] J. D. Jackson, *Classical Electrodynamics Third Edition*. Wiley, 1998.

[13] A. Pukhov, T. Baeva, D. An Der Brügge, and S. Münster, "Relativistic high harmonics and (sub-) attosecond pulses: relativistic spikes and relativistic mirror," *The European Physical Journal D*, vol. 55, no. 2, p. 407, 2009.

[14] C. Thaury and F. Quéré, "High-order harmonic and attosecond pulse generation on plasma mirrors: basic mechanisms," *Journal of Physics B: Atomic, Molecular and Optical Physics*, vol. 43, no. 21, p. 213001, 2010.

[15] A. D. Rakić, "Algorithm for the determination of intrinsic optical constants of metal films: application to aluminum," *Applied optics*, no. 22, pp. 4755–4767, 1995.

[16] G. D. Tsakiris, K. Eidmann, J. Meyer-ter Vehn, and F. Krausz, "Route to intense single attosecond pulses," *New Journal of Physics*, vol. 8, no. 1, p. 19, 2006.

[17] K. Budil, P. Salières, A. L'Huillier, T. Ditmire, and M. Perry, "Influence of ellipticity on harmonic generation," *Physical Review A*, vol. 48, no. 5, p. R3437, 1993.

[18] P. Corkum, N. Burnett, and M. Y. Ivanov, "Subfemtosecond pulses," *Optics letters*, vol. 19, no. 22, pp. 1870–1872, 1994.

[19] S. G. Rykovanov, M. Geissler, J. Meyer-ter Vehn, and G. D. Tsakiris, "Intense single attosecond pulses from surface harmonics using the polarization gating technique," *New Journal of Physics*, vol. 10, no. 2, p. 025025, 2008.

[20] R. Lichters, J. Meyer-ter Vehn, and A. Pukhov, "Short-pulse laser harmonics from oscillating plasma surfaces driven at relativistic intensity," *Physics of Plasmas*, vol. 3, no. 9, pp. 3425–3437, 1996.

[21] C. Heyl, S. Bengtsson, S. Carlström, J. Mauritsson, C. Arnold, and A. LHuillier, "Noncollinear optical gating," *New Journal of Physics*, vol. 16, no. 5, p. 052001, 2014.

[22] M. Louisy, C. Arnold, M. Miranda, E. W. Larsen, S. N. Bengtsson, D. Kroon, M. Kotur, D. Guénot, L. Rading, P. Rudawski *et al.*, "Gating attosecond pulses in a noncollinear geometry," *Optica*, vol. 2, no. 6, pp. 563–566, 2015.

[23] J. A. Wheeler, A. Borot, S. Monchocé, H. Vincenti, A. Ricci, A. Malvache, R. Lopez-Martens, and F. Quéré, "Attosecond lighthouses from plasma mirrors," *Nature Photonics*, vol. 6, no. 12, p. 829, 2012.

[24] C. Rödel, D. an der Brügge, J. Bierbach, M. Yeung, T. Hahn, B. Dromey, S. Herzer, S. Fuchs, A. G. Pour, E. Eckner *et al.*, "Harmonic generation from relativistic plasma surfaces in ultrasteep plasma density gradients," *Physical review letters*, vol. 109, no. 12, p. 125002, 2012.

[25] B. Dromey, S. Kar, C. Bellei, D. Carroll, R. Clarke, J. Green, S. Kneip, K. Markey, S. Nagel, P. Simpson *et al.*, "Bright multi-kev harmonic generation from relativistically oscillating plasma surfaces," *Physical Review Letters*, vol. 99, no. 8, p. 085001, 2007.